Asymmetrical temporal dynamics of topological edge modes in Su-Schrieffer-Heeger lattice with Kerr nonlinearity

Ghada Alharbi,[1,2] Stephan Wong,[1,3] Yongkang Gong,[1] and Sang Soon Oh[1,*]

[1]School of Physics and Astronomy, Cardiff University, Cardiff CF24 3AA, United Kingdom
[2]Department of Physics, University of Tabuk, Tabuk 741, Kingdom of Saudi Arabia
[3]Center for Integrated Nanotechnologies, Sandia National Laboratories, Albuquerque, New Mexico 87185, USA

(Dated: March 4, 2024)

Optical bistability and oscillating phases exist in a Sagnac interferometer and a single ring resonator made of $\chi^{(3)}$ nonlinear medium where the refractive indices are modulated by the light intensity due to the Kerr nonlinearity. An array of coupled nonlinear ring resonators behave similarly but with more complexity due to the presence of the additional couplings. Here, we theoretically demonstrate the bifurcation of topological edge modes which leads to optical bistability in the Su-Schrieffer-Heeger lattice with the Kerr nonlinearity. Additionally, we demonstrate periodic and chaotic switching behaviors in an oscillating phase resulting from the coupling between the topological edge mode and bulk modes with different chiralities, i.e., clockwise and counter-clockwise circulations.

I. INTRODUCTION

Asymmetrical states emerge when a system lose the balance and thus a symmetry between different components is broken. This can lead to bistability, where the system has two stable states for a single excitation. In some cases, asymmetrical dynamic states can emerge with periodic or chaotic oscillatory behaviors. In photonic systems, optical bistability can appear when the light transmits through a cavity with a nonlinear medium leading to two different optical states, where one mode is dominant (switched on) and the other is quenched (switched off) [1]. For instance, the stable symmetry breaking has been studied for counter-propagating light beams in a Sagnac interferometer [2] and micro-resonator with Kerr nonlinearity [3–7]. More interestingly, nonlinear optical ring resonators can present rich temporal dynamics with oscillatory behaviors, displaying various types of mode switching, such as chaotic, periodic, and self-switching dynamics [8]. These various dynamics are the result of the nonlinear interaction between the counter-propagating modes and they manifest the symmetry breaking, i.e., unequal intensities of the two counter-propagating modes.

Recently, topologically protected modes have been widely studied in photonic systems due to their intriguing properties, such as unidirectional light propagation and robustness to defects and disorders [9, 10]. In particular, topological edge modes in a one-dimensional (1D) Su-Schrieffer-Heeger (SSH) configuration and two-dimensional (2D) photonic quantum spin-Hall or quantum valley-Hall structures have been employed in an array of coupled lasers, namely topological lasers [11–16]. Moreover, nonlinear topological photonics has been studied in various platforms such as waveguide arrays [17–20], microcavity polariton systems [21] and optical resonators [22–28]. The phase diagrams of a nonlinear SSH model and nonlinear breathing kagome model were drawn for the nonlinear parameters and coupling coefficients between sites [26]. Also, the edge solitons have shown to be stable at any energy when the ratio between the weak and strong couplings falls below a critical value [29]. Up until now, however, no research has demonstrated spontaneous symmetry breaking coming from the nonlinear response for the edge modes in photonic topological insulators.

In this paper, we theoretically show that we can observe asymmetrical temporal dynamics, including optical bistabilities and oscillation phases for topological edge modes in a nonlinear 1D SSH model. The system consists of an array of coupled ring resonators with the Kerr nonlinearity. Using the Lugiato-Lefever equation [30] with additional nearest neighbor couplings, we demonstrate the optical bistability of the topological edge mode in the nonlinear SSH lattice. Finally, we use Poincaré section plots, composed of the maxima of the oscillating intensities, to display the oscillation phases featuring periodic and chaotic switching.

II. LINEAR SSH MODEL WITH TWO COUNTER-PROPAGATING MODES

We start by considering a linear SSH chain which does not have any resonance frequency shift coming from a nonlinearity. As shown in Fig. 1(a), the one-dimensional chain has $(N + 1)$ unit cells and every unit cell hosts two ring resonators; one on the sublattice A, and the other on the sublattice B. The $(N + 1)$-th unit cell has only one ring resonator that belongs to the sublattice A, resulting in $M = 2N + 1$ ring resonators in total. In photonics, this SSH model can be implemented by alternating the gap size between the ring resonators, resulting in different intra- and inter-cell coupling coefficients v and w (Fig. 1(b)). The coupled ring resonators are excited by two optical pumps with the same intensity, both

* Email:ohs2@cardiff.ac.uk

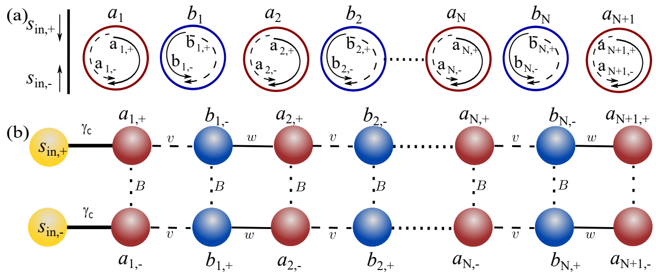

FIG. 1. (a) A 1D array of coupled ring resonators with alternating gap sizes. $s_{in,\pm}$ is the amplitude of input beams. (b) A schematic of the SSH model with resonators with Kerr nonlinearity. B is the XPM strength, v and w are the nearest neighbor coupling coefficients between ring resonators, and γ_c is the coupling coefficient between the waveguide and the first ring resonator.

of which are coupled into the first ring resonator but in the opposite directions exciting clockwise (CW) and counter-clockwise (CCW) modes, respectively. Then, the optical waves propagate back and forth through all the resonators via the couplings between the ring resonators. To calculate the intensities of circulating optical waves at all ring resonators, we describe the time evolution of the field amplitudes $a_n(t)$ and $b_n(t)$ in the n-th unit cell (Fig. 1(b)) for which we use the temporal coupled mode theory [31, 32]. Then, the coupled mode equations are written as:

$$\begin{aligned} \frac{da_{n,\pm}}{dt} &= i\Big(\omega_0 + i\gamma_n\Big)a_{n,\pm} + ivb_{n,\mp} + iwb_{n-1,\mp} \\ &\quad +\delta_{n,1}\gamma_c s_{in}, \\ \frac{db_{n,\pm}}{dt} &= i\Big(\omega_0 + i\gamma_n'\Big)b_{n,\pm} + iva_{n,\mp} + iwa_{n+1,\mp}, \end{aligned} \tag{1}$$

where

$$\begin{aligned} \gamma_n &= \gamma_0 + \delta_{n,1}\gamma_c, \\ \gamma_n' &= \gamma_0. \end{aligned} \tag{2}$$

Here, the subscript $\pm$ denotes the mode propagation directions, CW and CCW, respectively. $\delta_{n,1}$ is the Kronecker delta and ω_0 is the resonance frequency of the uncoupled ring resonators. The two input beams with the same amplitude s_{in}, which is given as $\sqrt{I_s}e^{i\omega t}$ for pump intensity I_s, are coupled to the CW and CCW modes in the first ring $(a_{1,\pm})$ with the waveguide-to-ring coupling coefficient γ_c. Note that only a_n's and b_n's are time-dependent functions and we have omitted the symbol (t) for brevity.

To be more compact, we express the coupled mode equations (Eq. (1)) in a matrix form by using the Hamiltonian $\mathbf{H}$ as

$$\frac{d\mathbf{x}}{dt} = \mathbf{H}\mathbf{x} + \mathbf{S} \tag{3}$$

where

$$\mathbf{x} = (a_{1,+}, b_{1,-}, a_{2,+}, b_{2,-}, \ldots, a_{1,-}, b_{1,+}, a_{2,-}, b_{2,+}, \ldots)^{\mathsf{T}}.$$

Note that the Hamiltonian $\mathbf{H}$ can be differently defined after multiplying i in both sides, which makes the equation look like the Schrödinger equation and makes its eigenvalues correspond to the real parts of the frequencies. However, we have chosen this notation to make Eq. (3) similar to Lugiato-Lefever equation which we will explain in the following section. Then, the Hamiltonian $\mathbf{H}$ can be split into two terms like:

$$\mathbf{H} = \mathbf{H}_0 + \mathbf{H}_c \tag{4}$$

where

$$\mathbf{H}_0 = i(\omega_0 + i\gamma_0)\mathbb{I}_M \tag{5}$$

with $\mathbb{I}_M$ the $(M \times M)$ identity matrix. The ring-to-ring coupling is expressed as:

$$\mathbf{H}_c = i\begin{pmatrix} 0 & v & 0 & 0 & \cdots \\ v & 0 & w & 0 & \cdots \\ 0 & w & 0 & v & \cdots \\ 0 & 0 & v & 0 & \cdots \\ \vdots & \vdots & \vdots & \vdots & \ddots \end{pmatrix}. \tag{6}$$

Finally, the source term $\mathbf{S}$ is expressed as $[s_{in,+}, 0, 0, \cdots, s_{in,-}, 0, 0, \cdots]^{\mathsf{T}}$. For the remainder of this paper, we assume the symmetric pumping by setting $s_{in,+} = s_{in,-}$.

The coupled mode equations (Eq. (3)) can be solved in both frequency and time domains. For example, in the frequency domain, by assuming $\mathbf{x} = \tilde{\mathbf{x}}\exp(i\omega t)$ and $\mathbf{S} = 0$, we obtain an eigenvalue equation

$$i\omega\tilde{\mathbf{x}} = \mathbf{H}\tilde{\mathbf{x}}. \tag{7}$$

Solving the eigenvalue equation gives an frequency spectrum with so-called zero-energy modes that are topologically protected and localized on one of the edges of the SSH chain with the smaller coupling coefficient among v and w. In this work, we will use the term *edge modes* because their frequencies deviate from the resonance frequency ω_0 and thus they are not any more zero-energy modes for nonlinear cases. We call the rest of the modes *bulk modes* as the mode fields are delocalized over the entire SSH lattice.

III. LUGIATO-LEFEVER EQUATION FOR NONLINEAR SSH MODEL

Now we introduce the Kerr nonlinearity in the linear SSH model. In optics, the Kerr nonlinearity induces various nonlinear effects, for instance, self-phase modulation (SPM), cross-phase modulation (XPM), four-wave mixing, and two-photon absorption [33]. Here, we only consider the SPM and XPM for the counter-propating rotating modes in the ring resonators, both of which lead to a shift of the resonance frequencies of the CW or CCW modes. Although only the couplings due to the XPM are shown in Fig. 1(b), the frequency shift $\Delta\omega$ is expressed by $(AI_{n,+} + BI_{n,-})$ where $I_{n,+}$ and $I_{n,-}$ are the intensities of the CW and CCW modes in the n-th ring resonator, respectively. A and B are the SPM and XPM nonlinear coefficients, respectively.

For simplicity, we use the normalized Lugiato-Lefever equation to describe the field amplitudes in our nonlinear SSH model [30]. Notably, the equation is equivalent to the one derived from the temporal coupled-mode theory (see the Appendix A for more details). With the time-varying envelope amplitudes $\tilde{a}(t)$, $\tilde{b}(t)$, defined as $a(t) = \tilde{a}(t)e^{i\omega t}$, $b(t) = \tilde{b}(t)e^{i\omega t}$ respectively, the Lugiato-Lefever equation for a 1D SSH array of nonlinear ring resonators can be written as:

$$\begin{aligned} \frac{d\tilde{a}_{n,\pm}}{d\bar{t}} &= -\tilde{a}_{n,\pm} - i\eta\Delta\tilde{a}_{n,\pm} + i\eta(A|\tilde{a}_{n,\pm}|^2 + B|\tilde{a}_{n,\mp}|^2)\tilde{a}_{n,\pm} \\ &\quad + iv\tilde{b}_{n\mp} + iw\tilde{b}_{n-1,\mp} + \delta_{n,1}s_{in}, \\ \frac{d\tilde{b}_{n,\pm}}{d\bar{t}} &= -\tilde{b}_{n,\pm} - i\eta\Delta\tilde{b}_{n,\pm} + i\eta(A|\tilde{b}_{n,\pm}|^2 + B|\tilde{b}_{n,\mp}|^2)\tilde{b}_{n,\pm} \\ &\quad + iv\tilde{a}_{n\mp} + iw\tilde{a}_{n+1,\mp}, \end{aligned} \tag{8}$$

where $\bar{t} = t\gamma_0$ is the dimensionless time. The first term on the right-hand side represents damping, while the second term stands for detuning ($\Delta = (\omega - \omega_0)/\gamma_0$), which is the difference between the frequency of the continuous wave input beams and the resonance frequency of a single ring resonator. The third and fourth terms correspond to the SPM and XPM, respectively, with the normalized nonlinear coefficients A and B, and $\eta = +1$ for a self-focusing medium or $\eta = -1$ for a self-defocusing medium. The terms with v and w refer to the intra- and inter-couplings between ring resonators as in the linear case. Finally, we add a nonlinear term to Eq. (4) to have the Hamiltonian for our nonlinear SSH model:

$$\mathbf{H} = \mathbf{H}_0 + \mathbf{H}_c + \mathbf{H}_{NL}, \tag{9}$$

where

$$\mathbf{H}_0 = -(1 + i\eta\Delta)\mathbb{I}_M, \tag{10}$$

and

$$\mathbf{H}_{NL} = i\eta\mathbb{I}_M \times \begin{pmatrix} A|\tilde{a}_{1,+}|^2 + B|\tilde{a}_{1,-}|^2 \\ A|\tilde{b}_{1,-}|^2 + B|\tilde{b}_{1,+}|^2 \\ A|\tilde{a}_{2,+}|^2 + B|\tilde{a}_{2,-}|^2 \\ A|\tilde{b}_{2,-}|^2 + B|\tilde{b}_{2,+}|^2 \\ \vdots \\ A|\tilde{a}_{1,-}|^2 + B|\tilde{a}_{1,+}|^2 \\ A|\tilde{b}_{1,+}|^2 + B|\tilde{b}_{1,-}|^2 \\ A|\tilde{a}_{2,-}|^2 + B|\tilde{a}_{2,+}|^2 \\ A|\tilde{b}_{2,+}|^2 + B|\tilde{b}_{2,-}|^2 \\ \vdots \end{pmatrix}. \tag{11}$$

To obtain the temporal evolution of the amplitudes for nonlinear SSH lattice, we can solve the time-dependent equation (Eq.(3)) with this Hamiltonian. However, we cannot solve the equation in the frequency domain by simply solviing an eigenvalue equation because it is a system of nonlinear equations.

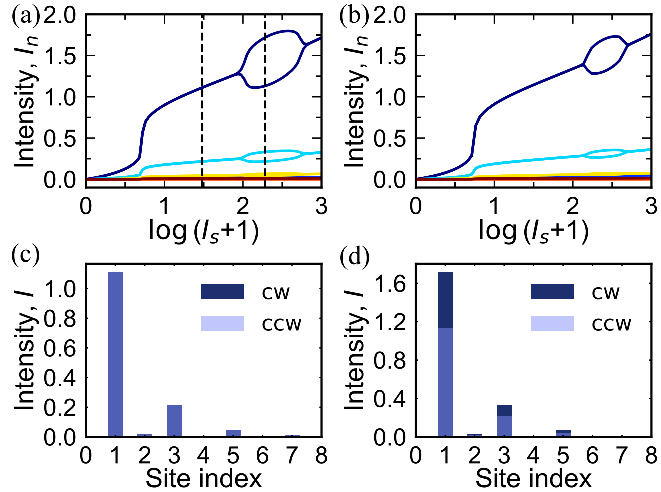

FIG. 2. (a) Optical bistability for seven ring resonators ($M = 7$) with detuning $\Delta = 1.85$, $v = 3$ and $w = 7$. (b) Optical bistability with the Kerr nonlinearity in the first ring resonator only. (c), (d) The distributions of intensity for the input intensities corresponding to the dashed vertical lines in (a)

IV. OPTICAL BISTABILITY OF TOPOLOGICAL EDGE MODES

Optical bistability in a single ring resonator is a result of the XPM between two counter-propagating modes [34]. This means that the Kerr nonlinearity leads to a shift in the resonance frequency of the two counter-propagating modes due to both SPM and XPM, and the coupling via XPM between them leads to spontaneous symmetry breaking above a certain threshold pump intensity [3]. Here, we want to address the question whether we can observe the optical bistability using an edge mode in a nonlinear SSH lattice model.

To theoretically observe the optical bistability in the nonlinear SSH lattice, we consider a SSH array of seven ring resonators ($M = 7$) with the nonlinear parameter and the detuning in Ref. [34] and the alternating coupling coefficients ($v = 3$ and $w = 7$). In our simulations, we scan the pump intensity I_s for a certain interval with random initial conditions. Indeed, as shown in Fig. 2(a), we observe the optical bistability in the range between $\log(I_s + 1) = 1.9$ and $\log(I_s + 1) = 2.9$ of pump intensity. Note that the field amplitudes are relatively large for odd sites only (sublattice A), and the intensity decreases exponentially along the right direction for both single stable (Fig. 2(c)) and bistable cases (Fig. 2 (d)), which is the reminiscence of the zero-energy edge modes.

To explain the origin of the observed optical bistabil-

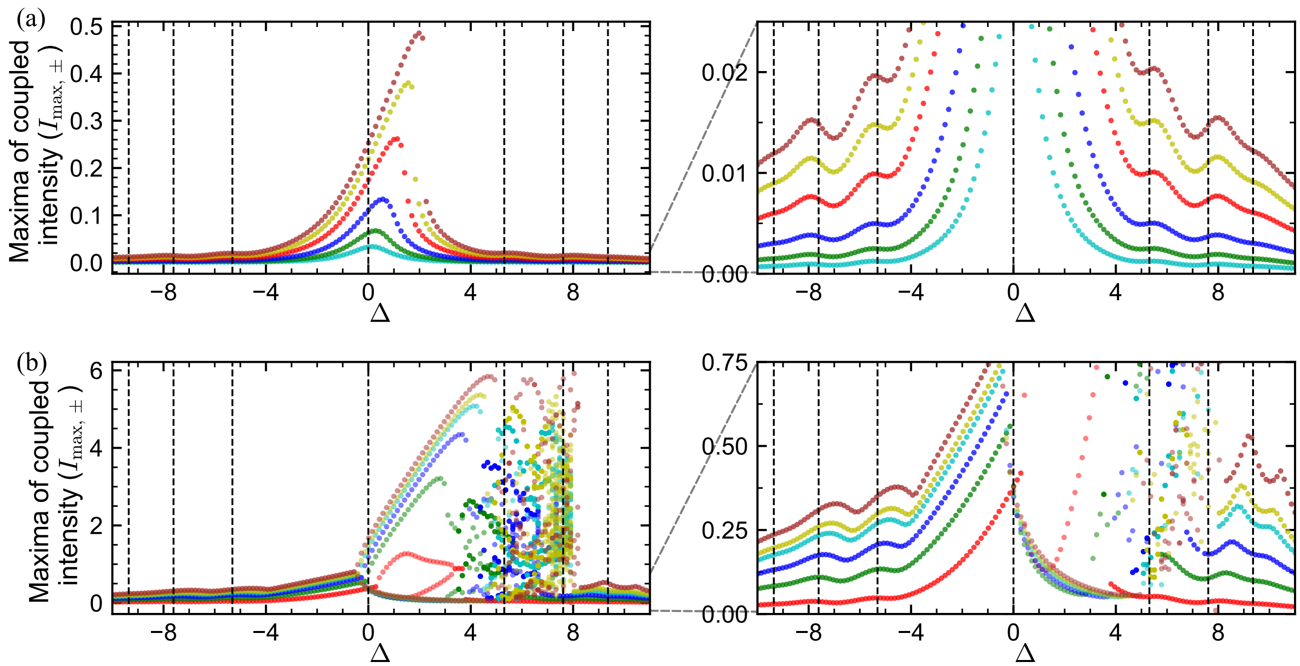

FIG. 3. Poincaré section of the maxima of the CW and CCW intensity time series for the first ring resonator in 1D SSH lattice composed seven ring resonators with alternating coupling, $v = 3$ and $w = 7$. (a) Maximum intensity curves for low input intensities $I_s = 0.05$ (cyan), 0.1 (green), 0.2 (blue), 0.4 (red), 0.6 (yellow), 0.8 (brown). (b) For high input intensities $I_s = 2$ (red), 6 (green), 10 (blue), 14 (cyan), 16 (yellow), 20 (brown), both optical bistability and oscillation regions appear. The vertical dashed lines indicate frequencies determined by the eigenvalue equation for the linear case (Eq.(7)).

ity, we hypothesize that the optical bistability comes from the symmetry breaking in the first ring only. First, optical bistability in a single ring resonator can occur when the pump intensity is above a certain threshold, called a bifurcation point. This means the first ring will show the optical bistability first as we increase the pump intensity under an excitation close to the zero-energy frequency. Indeed, the detuning $\Delta = 1.85$ is smaller than the topological band gap ($2|v-w| = 8$) meaning the zero-energy edge mode is dominantly excited even though it is off-resonance. This is supported by the field intensity distribution in Fig. 2(d). As the intensities in the rest of rings are much smaller than the first ring (Fig. 2(d)), only the first ring introduces bistability and the modes in the first ring couple to the other rings successively instead of having additional optical bistability from the rest of the rings. Second, to confirm this propagation, we consider the Kerr effect only in the first ring resonator but keep all other parameters the same. This is equivalent to switching off the Kerr effect in the $2N$ ring resonators except the first ring resonator in our original setting. As shown in Fig. 2(b), the intensity-intensity curve has almost identical shape as the original one except slight reduction in the range of I_s and slight change in the difference between two counter-propagating mode intensities.

V. ASYMMETRICAL TEMPORAL DYNAMICS

Now, let us look at the temporal evolution of the optical intensities of a 1D SSH array that contains seven ring resonators. To visualize oscillation and chaotic phases in our nonlinear system, we will use the Poincaré section obtained by plotting all the local maxima in a time series of oscillating intensities [8]. Since the intensity of each ring in the 1D SSH array follows the same pattern as the intensity of the first ring (see Fig. A1 in Appendix B), we plot the Poincaré sections for the first ring resonator only.

As shown in Fig. 3 (a)(b), the nonlinear SSH lattice exhibits both bistability and oscillation phases in the range of detuning corresponding to the edge mode and two bulk modes with positive detuning for the linear SSH lattice (denoted as the vertical dashed lines). Here, we set $A = 1$ and $B = 4$ and change the input intensity from 0.05 to 20 denoted with different colors. As we can see in the zoomed view of the plots, these spectra show seven resonance modes; one edge mode with the largest intensity in the middle and six bulk modes on both sides of the edge mode having three on each side. For low input intensities (Fig. 3(a)), the edge mode shifts dramatically and its intensity increases significantly, whereas the bulk modes shift less and their intensities increase slightly. This is due to the localization of intensity at the first ring resonator. For high input intensities (Fig. 3(b)), the CW

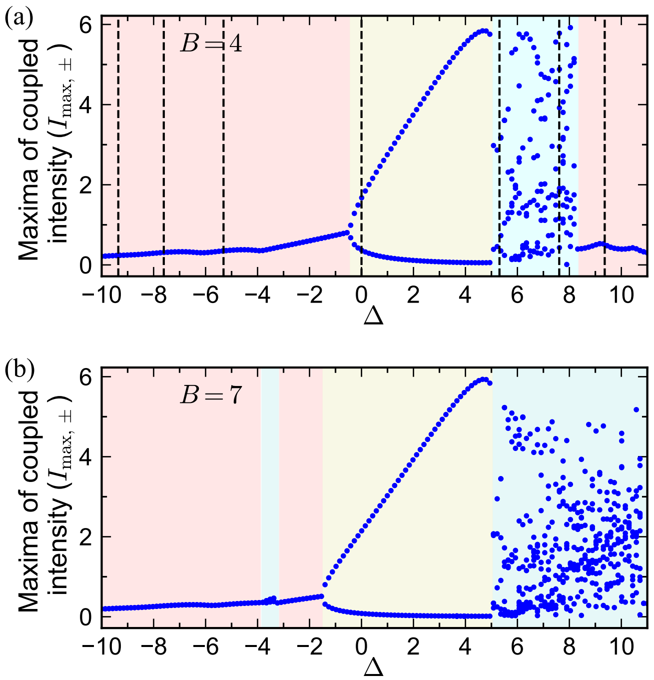

FIG. 4. Poincaré sections of the maxima of oscillating coupled intensity as a function of detuning for input intensity $I_s = 20$, for the first ring resonator from the 1D SSH array. The Poincaré sections for coupling coefficients ($v = 3$, $w = 7$) and XPM strength (B) of 4 and 7 in (a) and (b), respectively. The red shading indicates a symmetric case, the yellow indicates optical bistability, and the cyan indicates oscillations. The vertical dashed lines refer to resonance frequencies for the linear 1D SSH lattice.

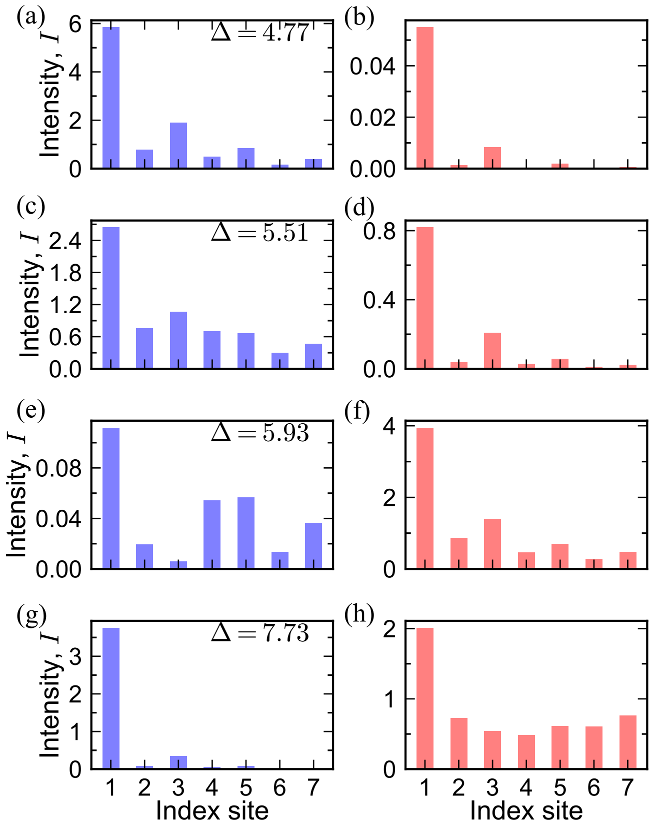

FIG. 5. Snapshots of intensity distribution in the nonlinear 1D SSH lattice for the CW modes in the left column and the CCW modes in the right column for different values of detuning with $I_s = 20$, $B = 4$.

and CCW modes for edge mode undergo an interaction between them via XPM, leading to an optical bistability. Remarkably, the high input intensity leads to the interaction between the edge mode and the bulk mode near $\Delta = 5.2$, resulting in a series of oscillation phases occurring for both CW and CCW modes.

The range of detuning of asymmetrical phases also depends on the XPM strength. Figure 4 (a) and (b) compare the Poincaré sections for two different values of XPM strength B. One can observe that increasing B leads to a larger range of detuning for asymmetrical phases including optical bistability (yellow) and oscillation phases (blue). The Poincaré section as a function of XPM strength can be found in Fig. A2 in Appendix C.

To better understand the asymmetrical dynamic modes, we show the spatial distributions and temporal changes of the excited mode intensity for different detuning in Fig. 5 and Fig. 6. Here, we focus on the case of $I_s = 20$ and $B = 4$ as an example of high input intensity. For the optical bistability ($\Delta = 4.77$) shown in Fig. 5(a),(b), both CW and CCW modes have contrasting intensity values, whereas their profiles are similar to the zero-energy edge mode's profile in a linear SSH model with exponentially decaying non-zero odd-site intensities and zero even-site intensities. The deviations can be attributed to the off-resonance excitation and the interaction between CW and CCW modes via the nonlinear process (XPM). Note that the excited mode is stable as they have constant intensities and appear as two separate points its phase space (Fig. 6 (a),(b)). When we increase the detuning further to $\Delta = 5.51$, both CW and CCW mode profile deviates further away from the zero-energy edge mode but the CCW mode profile deviates less still having low intensities at even sites (Fig. 5(c),(d)). Here, the largest value at the first site is related to the zero-energy edge mode and also due to the fact we are exciting the ring resonators from the waveguide on the left side. The dynamics for this detuning (Fig. 6 (c)(d)) is periodically oscillatory, resulting in two distinct regions in the phase space meaning the CW mode intensity is always larger than the CCW mode intensity (the trajectory for CW is further away from the origin). For slightly larger detuning of $\Delta = 5.93$, the two trajectories are merged into one meaning that the intensities between the two modes alternates. In the phase space, they are in different two points with the π phase difference in the same trajectory. For a large detuning of $\Delta = 7.73$, we see chaotic oscillations showing two separate trajectories covering a similar region in the phase space (Fig. 6(g),(h)).

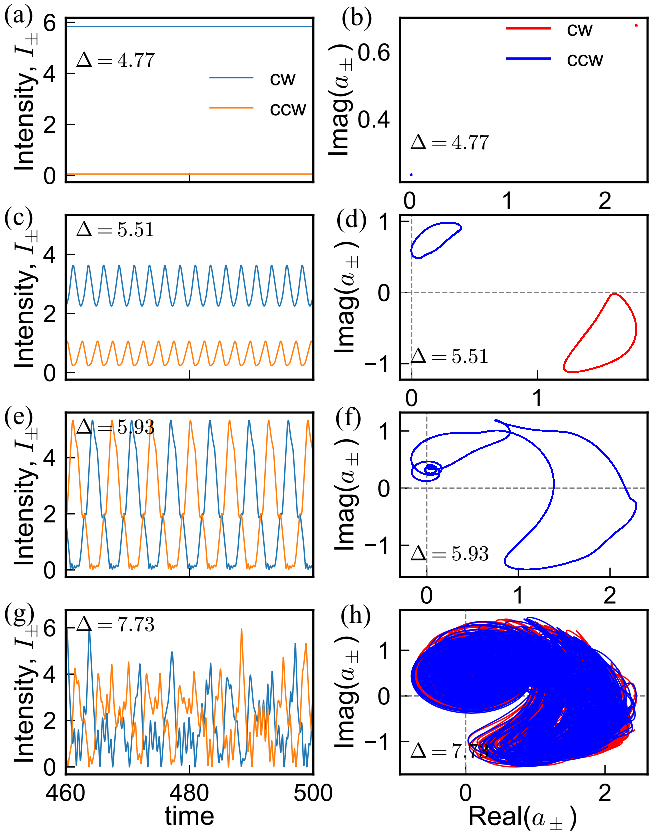

FIG. 6. Time series of intensity and their phase space trajectories for $A = 1$, $B = 4$ and $I_s = 20$ at different values of detuning, for the first ring resonators from 1 D SSH array of 7 rings. (a), (b) Optical bistability phase with $\Delta = 5.51$. (c), (d) Oscillations without overlapping trajectories. (e), (f) Periodic switching for $\Delta = 5.93$. (g), (h) Chaotic switching with $\Delta = 7.73$

In contrast to the optical bistability coming from the coupling between two counter-propagating modes via nonlinearity, the emergence of the periodic and chaotic oscillations come from the coupling between the edge mode and the bulk modes. The reasoning is below. First, the resonance frequency shift of the edge mode when increasing the intensity is much larger than the ones for the bulk modes as shown in Fig. 4. Second, although the intensity distributions for CW and CCW are close to the bulk modes, there are clear signatures of the edge modes, i.e., an exponentially decaying odd-site intensities and nearly zero even-site intensities (Fig. 5 (d)(f)(g)). Thus, our numerical simulations confirm that the edge mode overlap with bulk mode due to the Kerr nonlinearity results in the periodic and chaotic oscillations.

VI. CONCLUSIONS

In summary, we have numerically demonstrated the optical bistability and various types of oscillations in a 1D SSH model composed of ring resonators with Kerr nonlinearity. When the nonlinear terms are introduced in the Lugiato-Lefever equation, the first ring's CW and CCW mode intensities are symmetric until the pump intensity reaches a bifurcation point. Above the bifurcation point, the symmetry is spontaneously broken due to the splitting of the resonance frequencies of the two CW and CCW modes in the first ring resonator. For the high input intensity regime, we have observed oscillating phases including periodic and chaotic oscillations. The periodic oscillation phases can also be classified into two different phases where the trajectories are separate or identical in the phase space of the mode intensities. This emergence of the oscillating phases can be attributed to the coupling between the edge mode and bulk mode due to the large shift of resonance peaks of the edge mode.

We believe that our theoretical models and numerical results will provide valueable insight in understanding the complex dynamics in coupled nonlinear resonator systems with two chiral modes. Additionally, the various spatio-temporal dynamics could be applied to optical switching devices as well as the stability analysis of coupled lasers.

ACKNOWLEDGMENTS

We are grateful to Daniel Leykam for fruitful discussions. The work is part-funded by the European Regional Development Fund through the Welsh Government (80762-CU145 (East)).

Appendix A: Derivation of the Lugiato-Lefever equation using the coupled mode theory

The coupled mode theory [31] has been used to describe the field amplitude a propagating in an optical ring resonator, which can be written as

$$\frac{da}{dt} = i\omega_0 a - \gamma a + \gamma_c s. \tag{A1}$$

Here ω_0 refers to the resonance frequency, γ and γ_c are the damping and coupling with the source coefficient, respectively. we can express field amplitude a in terms of envelope amplitude $\tilde{a}$ as:

$$a = \tilde{a}e^{i\omega t}, \tag{A2}$$

by substituting in Eq.(A1) :

$$\frac{d\tilde{a}}{dt} = [i(\omega_0 - \omega) - \gamma]\tilde{a} + \gamma_c \tilde{s}, \tag{A3}$$

where $-\tilde{\Delta} = \omega_0 - \omega$, then we can rewrite this equation in terms of detuning as :

$$\frac{d\tilde{a}}{dt} = [-\gamma - i\tilde{\Delta}]\tilde{a} + \gamma_c \tilde{s}. \tag{A4}$$

This equation is equivalent to the Lugiato-Lefever equation without nonlinearity terms; the terms in RHS correspond to damping, detuning, and source terms, respectively.

Appendix B: Site-dependence of Poincaré sections for nonlinear SSH model

Figure A1 (a), (b) displays Poincaré sections of maxima of oscillating in coupled intensities $I_{max,\pm}$ for odd (sublattice A) and even (sublattice B) sites in the 1D SSH lattice, respectively. The odd-site intensities of the CW and CCW modes follow the same pattern as the ones for the first ring resonator, while the even-site intensities follow the same patter as the one the second ring resonator. The symmetry is broken, i.e., the CW and CCW mode intensities are notequal for the optical bistability and oscillation phases.

Appendix C: Poincaré sections of the maxima of oscillating coupled intensity as a function of B

In Fig. A2 we scan B from 1 to 7 to observe oscillations in coupled intensity for $A = 1$, $I_s = 20$, $v = 3$ and $w = 7$. Here, the Poincaré section can be divided into three regions: symmetric stable, asymmetric stable and asymmetric unstable states. We observe a series of bifurcations and oscillation windows for $B \geq 1.9$.

---

[1] R. W. Boyd, *Nonlinear Optics*, 3rd ed. (Academic Press, Inc, 2008).

[2] A. Kaplan and P. Meystre, Directionally asymmetrical bistability in a symmetrically pumped nonlinear ring interferometer, Optics Communications **40**, 229 (1982).

[3] L. Del Bino, J. M. Silver, S. L. Stebbings, and P. Del'Haye, Symmetry Breaking of Counter-Propagating Light in a Nonlinear Resonator, Scientific Reports **7**, 1 (2017).

[4] L. Del Bino, J. M. Silver, M. T. M. Woodley, S. L. Stebbings, X. Zhao, and P. Del'Haye, Microresonator isolators and circulators based on the intrinsic nonreciprocity of the Kerr effect, Optica **5**, 279 (2018).

[5] J.-B. Shim, P. Schlagheck, M. Hentschel, and J. Wiersig, Nonlinear dynamical tunneling of optical whispering gallery modes in the presence of a Kerr nonlinearity, Physical Review A **94**, 053849 (2016).

[6] G. Xu, A. U. Nielsen, B. Garbin, L. Hill, G. L. Oppo, J. Fatome, S. G. Murdoch, S. Coen, and M. Erkintalo, Spontaneous symmetry breaking of dissipative optical solitons in a two-component Kerr resonator, Nature Communications **12**, 4023 (2021).

[7] S. Coen, G. Xu, L. Quinn, B. Garbin, G.-L. Oppo, N. Goldman, S. G. Murdoch, M. Erkintalo, and J. Fatome, Nonlinear topological protection of spontaneous symmetry breaking in a driven Kerr resonator, in *Conference on Lasers and Electro-Optics*, Technical Digest Series (Optica Publishing Group, San Jose, California, 2022) p. JM3A.3.

[8] L. Hill, G.-L. Oppo, M. T. M. Woodley, and P. Del'Haye, Effects of self- and cross-phase modulation on the spontaneous symmetry breaking of light in ring resonators, Physical Review A **101**, 013823 (2020), 1905.01119.

[9] T. Ozawa, H. M. Price, A. Amo, N. Goldman, M. Hafezi, L. Lu, M. C. Rechtsman, D. Schuster, J. Simon, O. Zilberberg, and I. Carusotto, Topological photonics, Reviews of Modern Physics **91**, 015006 (2019).

[10] A. B. Khanikaev, S. Hossein Mousavi, W.-K. Tse, M. Kargarian, A. H. MacDonald, and G. Shvets, Photonic topological insulators, Nature Materials **12**, 233 (2013).

[11] J. Noh, S. Huang, K. P. Chen, and M. C. Rechtsman, Observation of Photonic Topological Valley Hall Edge States, Physical Review Letters **120**, 063902 (2018).

[12] C. Han, M. Lee, S. Callard, C. Seassal, and H. Jeon, Lasing at topological edge states in a photonic crystal L3 nanocavity dimer array, Light: Science & Applications **8**, 40 (2019).

[13] G. Harari, M. A. Bandres, Y. Lumer, M. C. Rechtsman, Y. D. Chong, M. Khajavikhan, D. N. Christodoulides, and M. Segev, Topological insulator laser: Theory, Science **359**, eaar4003 (2018).

[14] M. A. Bandres, S. Wittek, G. Harari, M. Parto, J. Ren, M. Segev, D. N. Christodoulides, and M. Khajavikhan, Topological insulator laser: Experiments, Science **359**, eaar4005 (2018).

[15] Y. Gong, S. Wong, A. J. Bennett, D. L. Huffaker, and S. S. Oh, Topological Insulator Laser Using Valley-Hall Photonic Crystals, ACS Photonics **7**, 2089 (2020).

[16] S. Wong, J. Olthaus, T. K. Bracht, D. E. Reiter, and S. S. Oh, A machine learning approach to drawing phase diagrams of topological lasing modes, Communications Physics **6**, 104 (2023).

[17] D. Leykam and Y. D. Chong, Edge Solitons in Nonlinear-Photonic Topological Insulators, Physical Review Letters **117**, 143901 (2016).

[18] X. Zhou, Y. Wang, D. Leykam, and Y. Chong, Optical isolation with nonlinear topological photonics, New Journal of Physics **19**, 095002 (2017).

[19] L. J. Maczewsky, M. Heinrich, M. Kremer, S. K. Ivanov, M. Ehrhardt, F. Martinez, Y. V. Kartashov, V. V. Konotop, L. Torner, D. Bauer, and A. Szameit, Nonlinearity-induced photonic topological insulator, Science **370**, 701 (2020), 2010.12250.

[20] S. K. Ivanov, Y. V. Kartashov, and L. Torner, Light bullets in Su-Schrieffer-Heeger photonic topological insulators, Physical Review A **107**, 033514 (2023).

[21] Y. V. Kartashov and D. V. Skryabin, Bistable Topological Insulator with Exciton-Polaritons, Physical Review Letters **119**, 253904 (2017).

[22] Y. Hadad, A. B. Khanikaev, and A. Alù, Self-induced topological transitions and edge states supported by nonlinear staggered potentials, Physical Review B **93**, 155112 (2016).

[23] D. A. Dobrykh, A. V. Yulin, A. P. Slobozhanyuk, A. N. Poddubny, and Y. S. Kivshar, Nonlinear Control of Elec-

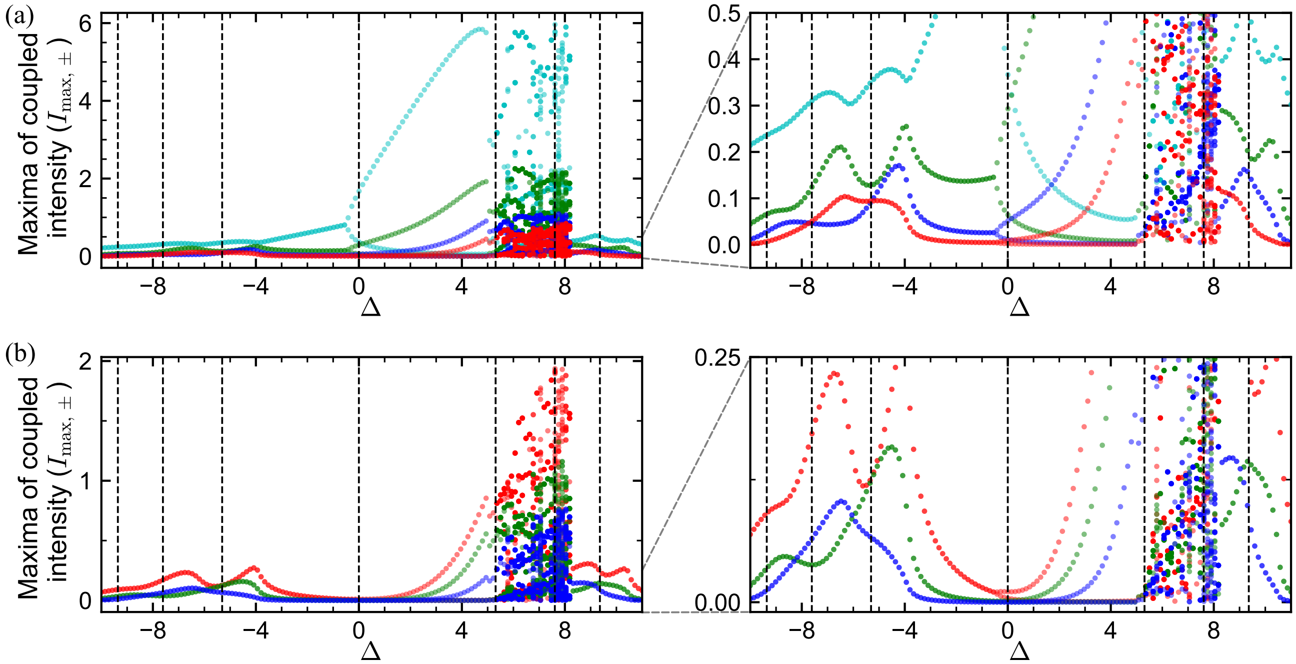

FIG. A1. Poincaré sections of the maxima of oscillating coupled intensity as a function of detuning for a 1D SSH lattice ($M = 7$) with the same parameters in Fig. 4. (a) For odd sites in the main text ($I_s = 20, v = 3, w = 7, A = 1, B = 4$) with the cyan, green, blue, and red colors corresponding to the 1st, 3rd, 5th, and 7th ring resonators respectively. (b) For even sites with the red, green and blue colors corresponding to the 2nd, 4th, and 6th ring resonators, respectively.

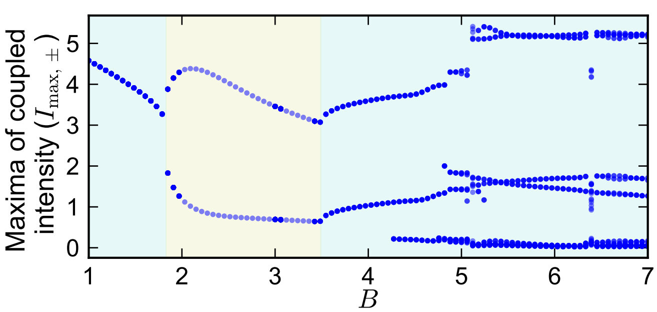

FIG. A2. Poincaré section of the maxima of oscillating coupled intensity as a function of B for input intensity $I_s = 20$, for the first ring resonator from the 1D SSH array. The Poincaré sections for coupling coefficients ($v = 3$, $w = 7$) and $\Delta = 5.5$. Cyan shading indicates oscillations and yellow refers to optical bistability.

tromagnetic Topological Edge States, Physical Review Letters **121**, 163901 (2018).

[24] D. Leykam and L. Yuan, Topological phases in ring resonators: recent progress and future prospects, Nanophotonics **9**, 4473 (2020), 2007.11807.

[25] A. Roy, M. Parto, R. Nehra, C. Leefmans, and A. Marandi, Topological optical parametric oscillation, Nanophotonics **11**, 1611 (2022), 2108.01287.

[26] M. Ezawa, Nonlinearity-induced transition in the nonlinear Su-Schrieffer-Heeger model and a nonlinear higher-order topological system, Physical Review B **104**, 235420 (2021).

[27] M. Ezawa, Nonlinear non-Hermitian higher-order topological laser, Physical Review Research **4**, 013195 (2022).

[28] M.-S. Wei, M.-J. Liao, C. Wang, C. Zhu, J. Xu, and Y. Yang, Phase transition and dynamics of qubits in coupled-cavity arrays with nonlinear topological photonics, Results in Physics **45**, 106232 (2023).

[29] Y.-P. Ma and H. Susanto, Topological edge solitons and their stability in a nonlinear Su-Schrieffer-Heeger model, Physical Review E **104**, 054206 (2021).

[30] L. A. Lugiato and R. Lefever, Spatial Dissipative Structures in Passive Optical Systems, Physical Review Letters **58**, 2209 (1987).

[31] H. H. Haus, *Waves and Fields in Optoelectronics* (Prentice Hall, 1983).

[32] W. Suh, Z. Wang, and S. Fan, Temporal coupled-mode theory and the presence of non-orthogonal modes in lossless multimode cavities, IEEE J. Quantum Electron. **40**, 1511 (2004).

[33] G. Agrawal, *Nonlinear fiber optics*, sixth ed. (Academic Press, London, England, 2019).

[34] A. E. Kaplan and P. Meystre, Enhancement of the Sagnac effect due to nonlinearly induced nonreciprocity, Optics Letters **6**, 590 (1981).